Preparation of graphene/TiO$_2$ nanotube arrays photoelectrodes and their photocatalytic activities for the degradation of alachlor

Dong Zheng[a, b], Yanjun Xin[a, c], Dong Ma[a, c], Xu Wang[a], Juan Wu[c], Mengchun Gao[a,*]

[a] *Key Lab of Marine Environmental Science and Ecology, Ministry of Education, Ocean University of China, Qingdao 266100, China*

[b] *College of Environmental Science and Engineering, Ocean University of China, Qingdao 266100, China*

[c] *College of Resource and Environment, Qingdao Agricultural University, Qingdao 266109, China*

*Corresponding author.

Address: College of Environmental Science and Engineering, Ocean University of China, No. 238 Songling Road, Qingdao, Shandong Province 266100, China

Tel.: +86 532 66781061; **fax:** +86 532 66782810

E-mail address: mengchungao@outlook.com (M.C. Gao)

Abstract

Graphene/TiO$_2$ nanotube arrays (GR/TNAs) photoelectrodes were fabricated by combining in-situ anodization and electro-deposition process. The scanning electron microscopy (SEM), X-ray diffraction (XRD), Fourier transform infrared spectroscopy (FTIR), UV-vis diffuse reflectance spectra (DRS), photopotential measurement, electrochemical impedance spectroscopy (EIS) and zeta-potential measurement were employed to characterize the as-prepared samples. The photocatalytic properties of GR/TNAs photoelectrodes were investigated using the degradation of alachlor as a model reaction. The introduction of GR had no obvious effect on the original crystallization of TNAs, whereas the photoelectric property was significantly improved. The GR/TNAs photoelectrodes exhibited higher photocatalytic activity for the alachlor degradation than the bare TNAs photoelectrodes. The degradation efficiency of alachlor by GR/TNAs photoelectrodes gradually decreased with the increase of initial alachlor concentration, initial pH and distance from illuminant. Some interfering anions (e.g. NO$_3^-$ and SO$_4^{2-}$) could improve the photocatalysis efficiency, whereas Cl$^-$ exhibited a slight inhibition effect on the alachlor degradation. Additionally, GR/TNAs photoelectrodes possessed superb stability for maintaining as high alachlor degradation efficiency as more than 99.5% after the successive use of 15 times with 60 min irradiation for each cycle.

Keywords: GR/TNAs; Anodization; Electro-deposition; Photocatalysis; Alachlor

2

1. Introduction

As a typical herbicide, alachlor (2-chloro-2', 6'-diethyl N-methoxymethyl acetanilide) has been widely used in agriculture to control the growth of annual grasses and broadleaf weeds[1]. Due to the significant usage, alachlor can be released to the nature environment like soil and water, and it results in a noteworthy environmental issue and a threat to public health[2]. As alachlor is highly toxic and mutagenic to many organisms with moderate persistence, it is classified as a group B2 carcinogen by the U.S. Environmental Protection Agency[3, 4]. Therefore, the conventional biological technologies are not suitable for the treatment of wastewater containing alachlor and alternative remediation methods are required to remove alachlor with high efficiency.

Alachlor has been reported that it can be degraded by gamma radiolysis[5], photo-Fenton[6], ultrasonic[7] and photocatalysis[8]. Due to the safety, low-cost, relative high activity and long-term stability of photocatalysis, a photocatalysis process employing TiO_2 photocatalyst has become an appealing option for the degradation of refractory organics[9-11]. However, the further application of TiO_2 is limited by wide band gap, photoactivation confined to the UV region ($\lambda < 380$ nm), fast recombination of photo-generated electron-hole pairs[12, 13]. In order to resolve the above-mentioned problems, some technologies have been employed to improve the TiO_2 application in photocatalysis, including doping with metallic or non-metallic elements, modifying catalysts with noble metals or semiconductors and surface photosensitization[14, 15].

Graphene (GR), a two-dimensional carbonaceous material with atoms adapted in a honeycomb structure, has been widely used in electronic device, sensor and

composite with its superior mechanical, electrical and thermal properties[16, 17]. GR has

aroused wide concern in photocatalysis owing to its superior conductive ability, high

mobility, large specific surface area and strong adsorptivity toward organics[18-21].

Some researchers reported that the introduction of GR to TiO_2 could significantly

improve the photocatalytic property of TiO_2 for organic pollutant degradation[18, 22].

Similarly, previous reports have also found that the relatively higher GR ratio in the

GR/TiO_2 composites could favor the photodegradation properties, whereas the

excessive GR in the composites decreased the photocatalytic efficiency[12, 13]. In

addition, TiO_2 nanotube arrays (TNAs) can offer larger surface area, higher quantum

efficiency and excellent reusability without secondary pollution compared to the

randomly oriented TiO_2 nanoparticles, and the doping of GR on TNAs could improve

photocatalytic properties of TiO_2[23, 24]. The photocatalytic activity of GR/TNAs

photoelectrodes has been investigated in previous researches. However, most of these

researches chose the dyes or simple substance as target pollutants[14, 16, 25], such as

methylene blue, Rhodamine B and acid orange. Due to the overuse of alachlor, the

potential toxicity of alachlor has aroused public attention in China. To the best of our

knowledge, there is little study focusing on the modification of TNAs with GR and

the photocatalytic performance of GR/TNAs photoelectrodes for alachlor degradation.

The major objectives of the present study were (1) to prepared the GR/TNAs

photoelectrodes, (2) to characterize the morphology and structure of GR/TNAs

photoelectrodes, (3) to investigate the optical, electrochemical, photoelectric and

photocatalytic properties of GR/TNAs photoelectrodes, (4) to explore the effect of the

initial concentration of alachlor, pH value, distance from illuminant and interfering

anions on the alachlor degradation by GR/TNAs photoelectrodes, (5) to evaluate the

chemical stability of as-prepared GR/TNAs photoelectrodes.

2. Experimental

2.1. Chemicals and materials

Titanium foils (99.8%) were purchased from Baoji Titanium and Nickel Manufacture

Co., Ltd. Alachlor was purchased from Sigma–Aldrich Laborchemikalien Company.

The structure of alachlor is shown in Fig. 1. GR powders, sodium sulfate (Na_2SO_4),

sodium fluoride (NaF) and other reagents were obtained from Sinopharm Chemical

Reagent Co., Ltd. All reagents were of analytical grade and used without further

purification. Aqueous solutions in experiments were prepared by employing deionized

water.

2.2. Pretreatment of Ti foils

Prior to the preparation of TNAs, Ti foils were pretreated as follows[14]: (1) The dense

titanium oxide film on the surface of the Ti sheets were removed by using the acid

mixture of hydrofluoric acid and concentrated nitric acid (1:1). The sample was

subsequently rinsed with deionized water and dried at room temperature; (2) The Ti

slices were sanded and polished by using sandpapers with different mesh of 260, 400,

600, 1000 and 2000 for one time, respectively; (3) The polished Ti sheets were

successively exposed in the deionized water and the mixed solution of ethanol and

acetone (1:1) for ultrasonic cleaning, and the subsequent ultrasonic cleaning was

performed in deionized water again. The samples were finally dried at room temperature.

2.3. Preparation of TNAs electrodes

The highly ordered TNAs electrodes were fabricated by in-situ anodization method[26]. Ti sheet and platinum (Pt) foil were served as the anode and cathode, respectively, and Ti foils were anodized in the aqueous solution containing 0.5% NaF and 1 M Na_2SO_4 with a constant potential of 20 V for 2 h. The effective area of electrodes exposed to the electrolytes was about 10 mm×20 mm. The as-prepared TNAs samples were rinsed by deionized water and dried at room temperature in air, followed by annealing at 550 ℃ for 2 h in a muffle furnace.

2.4. Preparation of GR/TNAs photoelectrodes

Graphene oxide (GO) was synthesized in the laboratory from graphite powder according to the modified Hummers method[27, 28], and subsequent ultrasonic treatment with GO was conducted to obtain the GO dispersion[29]. GR was further obtained by the electro-reduction process and GR/TNAs photoelectrode was synthesized by electro-deposition method on the surface of TNAs. Pt foil was used as the positive electrode while the as-prepared TNAs photoelectrode was served as the counter electrode. The preparation parameters in the present study were fixed at 2 cm electrode spacing, 80 mg/L GO dispersion, 2 V deposition voltage and 2 min deposition time.

2.5. Photocatalytic degradation of alachlor

The experiment of photocatalytic degradation on alachlor was carried out in a quartz

beaker containing 30 mL of 5 mg/L alachlor solution with a magnetic stirrer. The

as-prepared GR/TNAs photoelectrodes were placed vertically in the reactor and xenon

light was employed as the simulated light source. The samples were measured by

Waters 600E-2487 high performance liquid chromatography (HPLC), and the

chromatographic conditions were shown as follows: (1) chromatogram column:

KromasiIKR 100-5C18 chromatographic column (AKZONOBEL, USA); (2) mobile

phase: acetonitrile/water (V/V)=7:3; (3) flow rate: 1.0 mL/min; (4) column

temperature: 35℃; (5) determine wavelength: 200 nm. The calculation of degradation

efficiency was referred to following equation:

$$R(\%) = \frac{C_0 - C_t}{C_0} \times 100\% \tag{1}$$

where R represents the degradation efficiency of alachlor, C_0 is the alachlor

concentration of ad-desorption equilibrium, and C_t is the alachlor concentration at

irradiation time t.

2.6. Characterization

The morphology and structure of the photoelectrodes surface were acquired by using

SEM (QUANTA200F, FEI, USA). The XRD patterns were obtained by using a

D/max-γB X-ray diffractometer (Rigaku, Japan) over the 2θ range 10-90° with Cu Kα

radiation to characterize the crystal structures. The analysis of molecular structure and

the identification of the functional group of the sample were carried out with FTIR

spectrometer (Tensor 27, Bruker Optics, Germany.) using KBr disks. UV-vis DRS

were recorded on a TU1901 UV-vis spectrophotometer (Purkinje General Instrument

Co., Ltd, Beijing), in which $BaSO_4$ was employed as the reference. Zeta-potential of

the photoelectrodes were determined on a JS94H micro-electrophoresis apparatus

(Zhongchen digital technic apparatus Co.,Ltd, Shanghai). Photopotential measurement

and EIS were carried out via an electrochemical workstation (AutoLab, Metrohm) in a

three-electrode cell using a Pt plate, saturated calomel electrode (SCE) and the

as-prepared photoelectrodes as the counter electrode, reference electrode and working

electrode, respectively. The 0.5 M Na_2SO_4 aqueous solution was employed as

electrolyte and a 150 W xenon lamp was used as the illuminant positioned 3 cm away

from the photoelectrodes.

3. Results and discussion

3.1. Characterization of GR/TNAs photoelectrodes

The morphology and structure of the as-prepared GO, TNAs and GT/TNAs

photoelectrodes were characterized by SEM. As shown in Fig. 2a and 2b, the GO was

transparent and corrugated with a layered structure, and the TNAs presented a tubular

structure with uniform and high-density characteristics on the surface of Ti foil. The

average inner diameter and wall thickness of the tube in the TNAs were estimated

about 100 nm and 10 nm, respectively. The continuous and transparent islands of GR

were clearly observed on the top surface of TNAs (Fig. 2c), which indicated that the

GR sheets were successfully attached to the TNAs after electro-deposition treatment.

The XRD pattern was performed to determine the crystalline structures of the

raw graphite, GO, TNAs and GR/TNAs (Fig. 3). The dominant peak at 26.43° relating

to (002) lattice plane in the graphite disappeared during the oxidization of graphite to

GO, whereas a strong diffraction (001) peak centered at 10.29° appeared in the curve

of GO. The calculation results of the Bragg equation illustrated that the average

interlayer distances of the GO was 5.23 Å more than and that of raw graphite due to

the intercalation of oxygen-containing groups into the stacked GO layers. As shown in

Fig. 3, the characteristic peak of GO at 10.29˚ disappeared with the successful

reduction of GO to GR. No diffraction peak of GR was found in the GR/TNAs, which

could be attributed to a smaller fraction of the GR in the GR/TNAs or the overlap of

diffraction peak in the GR at around 25.0˚ and the (101) peak in the anatase TiO_2[28].

The diffraction peaks of anatase TiO_2 (JCPDS No. 21-1272) at 25.3˚ and 48˚ in the

TNAs pattern were assigned to the (101) and (200) crystal planes, respectively[12].

Likewise, the diffraction peaks of rutile TiO_2 (JCPDS No. 76-1940) at 27.5˚ was

related to the (110) crystal planes. Both the GR/TNAs and TNAs could have the

similar crystal structure due to their similar XRD patterns, suggesting that the

introduction of GR didn't cause oblivious variation for the original crystal phase of

TNAs.

Fig. 4a shows the XPS spectra of all elements on the surface of GO, GR, TNAs

and GR/TNAs photoelectrodes. No peak for Ti 2p was found in the XPS spectra of

GO and GR. Similarly, no impurity was found from the XPS spectra of GO, GR,

TANs and GR/TNAs photoelectrodes. The oxygen contents of GO and GR were 61.2%

and 25.8%, respectively, which could conclude that some oxygen-containing

functional groups were removed during the reduction process of GO. As shown in Fig.

4b, the high-resolution C 1s XPS spectra of GR/TANs photoelectrodes were

compared with that of GO. The C 1s in the GO were divided into four sub-peaks as

follows: (1) the C-O in C-OH groups at 286.9 eV; (2) the carbonyl C in C=O at 287.8

eV; (3) the carboxylate carbon in O=C-OH at 288.9 eV; and (4) the non-oxygenated

ring C at 284.6 eV[30]. In addition to the non-oxygenated ring C, the intensity of the

above-mentioned peaks in the GR/TANs photoelectrodes sharply decreased compared

to the GO, which could further explain the reduction process of the GO to the GR.

The high-resolution Ti 2p XPS spectra of TANs were divided into two sub-peaks (Fig.

4c), including Ti $2p_{3/2}$ at around 458.4 eV and Ti $2p_{1/2}$ at around 464.2 eV, which were

in good agreement with the binding energy values of the Ti^{4+} oxidation state[31].

Compared with the pure TNAs, the slight shifts in the Ti $2p_{3/2}$ and Ti $2p_{1/2}$ peaks were

observed in the GR/TNAs photoelectrodes, suggesting there was a weak electronic

interaction between the GR and the TNAs. Fig. 3d shows the high-resolution O 1s

XPS spectra of TNAs and GR/TNAs photoelectrodes. The peaks centered at 529.5

and 531.1 eV in the high-resolution O 1s XPS spectra of TNAs were identified as the

surface lattice oxygen (O_{latt}) and adsorbed oxygen (O_{ads}) species, respectively[32]. The

higher amount of O_{ads} species (O^-, O_2^- or O_2^{2-}) in the GR/TNAs photoelectrodes

meant a higher oxygen vacancy density, which played an important role in the

photocatalytic process. The molar ratio of O_{ads}/O_{latt} for the GR/TNAs photoelectrodes

was about 1.5 times higher than that of pure TNAs, which could lead to better

photocatalytic performance for the GR/TNAs photoelectrodes.

The characteristic FTIR spectra of graphite, GO, TNAs and GR/TNAs are shown in Fig. 5. The intensity of peak centered at 1602 cm^{-1} was very low in the FTIR spectrum of graphite owing to the C=C vibration in the sp^2 domains. The peaks located at 1735 cm^{-1}, 1402 cm^{-1}, 1226 cm^{-1} and 1053 cm^{-1} in the FTIR spectra of GO were related to the C=O stretching vibration of ketones, O-H deformation vibration of C-OH groups, C-O-C vibration of epoxide and C-O stretching vibration of carboxylates, respectively[29, 33]. The broad peak centered at 3421 cm^{-1} was assigned to the -OH stretching vibrations of the C-OH groups and water[34]. The absorption band around 1623 cm^{-1} was related to C=C ring stretching or H-O-H bending band of the adsorbed H$_2$O molecules[35]. The FTIR spectra revealed the intercalating of a large amount of oxygen containing group into graphite after the treatment by using the modified Hummers method. However, many absorption bands relating to the oxygen functional groups of GO disappeared in the FTIR spectra of GR/TNAs. The intensities of the peaks at 3421 cm^{-1} and 1623 cm^{-1} in the FTIR spectra of both TNAs and GR/TNAs were weaker than those in the FTIR spectra of GO, which could be speculated that the H$_2$O molecule on the surface of TNAs could induce the O-H stretching vibration and the H-O-H bending vibration[36, 37].

Fig. 4 shows the UV-vis DRS of TNAs and GR/TNAs photoelectrodes. TNAs presented intrinsic band-gap absorption within the range of 200-400 nm accompanied by the mild light response within 400-500 nm[38]. According to the report of Zhuang et al.[39], the peak appeared in the range of 400-500 nm could be ascribed to the structure defect absorption of TiO$_2$. The trapped hole exhibited the absorption at wavelength

around 430 nm or shorter, and the trapped electron showed the absorption at about

500 nm, which could contribute the visible light absorption for the GR/TNAs

photoelectrodes. The introduction of GR into the matrix of TNAs caused some

obvious improvements of light absorption intensity in both visible and UV light

regions. The absorption edge of GR/TNAs had a red shift compared to the naked

TNAs. The above-mentioned results revealed that the energy levels of TNAs might be

rearranged during the GR doping process[40], and it could be explained as follows: The

oxygen containing groups such as -OH, C=O and C-O-C were removed from the

surface of GO after the treatment of electro-deposition, and the π electron residue of

carbon formed the delocalized large π bond. The unpaired π electrons could be

interacted with the Ti atoms and O atoms to form the Ti-O-C structure, leading to the

shifting up of the valence band and the narrowing of the band gap[13, 28, 41]. The UV-vis

DRS indicated that the addition of GR to TNAs could enhance the light absorption

efficiency and photocatalytic activity of TNAs.

The photovoltage measurement and EIS were used to investigate the

photoelectrochemical property of the as-synthesized photoelectrodes. As shown in Fig.

7, both the TNAs and GR/TNAs exhibited a sharp and uniform response to each

ON-OFF light cycle. Before switching on the light source, the open-circuit voltages of

TNAs and GR/TNAs photoelectrodes maintained at -97 mV and -70 mV, respectively.

Compared to the TNAs, the introduction of GR led to a relatively low initial potential

of GR/TN. The illumination induced the generation of excited photoelectrons and led

to the electron transition and accumulation on the conduction band of TNAs after

switching on the light source[42], which caused a rapid increase in the photovoltages of both the TNAs and GR/TNAs. The photovoltage response of GR/TNAs was higher than that of TNAs due to the superior property of GR in capturing and conducting charge carriers[19]. The electrons generated from TNAs could be efficiently captured in the GR/TNAs system by the two-dimensional π-π conjugation structure of GR, and the GR served as the transporter to promptly drive the charge to the external circuit[40]. The addition of GR contributed to a higher efficiency of charge separation and suppressed the recombination of photo-induced electro-hole pairs, resulting in the enhancement on the photovoltage response of GR/TNAs[29, 43]. When the illumination was cut off, the accumulated electrons during the switch-on event could be transferred to the solution, the back contact or the surface states[44]. The recovery of the potential for GR/TNAs photoelectrodes was more sensitive than that for TNAs. Both the patterns of TNAs and GR/TNAs kept stable after the first ON-OFF cycle, which might benefit from the ordered structure of TNAs.

As shown in Fig. 8, the EIS measurements in the darkness and xenon light illumination were used to determine the interfacial property of TNAs and GR/TNAs photoelectrodes. The equivalent circuit proposed for GR/TNAs and TNAs photoelectrodes in the dark and under illumination were depicted in Fig. 9. In the equivalent circuit, R_s represents the solution resistance and the uncompensated potential drop. R_n and Q_1 are the resistance and capacitance of the solid-state interface layer, respectively, resulting from the passivation reaction between the electrode surface and electrolyte. R_{ct} and Q_2 are the charge transfer resistance and the

double-layer capacitance on the photoelectorde, respectively. W is the Warburg

impedance arising from the mass transfer from the bulk of the electrolyte to the

reaction site[44]. The EIS Nyquist plots of both the TNAs and GR/TNAs exhibited

straight slopping lines without illumination in the range of the whole frequency,

suggesting that the electron-transfer process might be limited in darkness. However,

both the TNAs and GR/TNAs displayed two depressed semicircles in the plots at high

frequency under the xenon light illumination, and the introduction of GR significantly

reduced the semicircle size compared to the pure TNAs. Some researches reported

that the charge-transfer limiting process was caused by the double-layer capacitance

and charge transfer resistance, and it could be evaluated by the diameter of the

high-frequency arc in the EIS Nynquist plot[43, 45, 46]. The smaller semicircle in the plot

of GR/TNAs revealed a decrease in the resistance of the solid state interface layer and

the solid-liquid junction, which could significantly accelerate the electron migration

process corresponding to the results of photovoltage measurement[47, 48]. The present

results illustrated that the hybrid structures of the GR/TNAs could enhance the ability

of TNAs on electron accepting and transferring, and improved the photocatalytic

efficiency.

As the cation and anion could affect the catalytic performance of GR/TNAs

photoelectrodes, the surface charge of GR/TNAs was detected by

micro-electrophoresis apparatus. As shown in Fig. 8, the zeta potential value of

GR/TNAs switched from positive zeta potential (+39 mV) to negative zeta potential

(-35 mV) with the increase of pH value from 1 to 12. These results in the present

study suggested that the surface charge of GR/TNAs photoelectrodes could be

significantly affected by the change of the pH value, and the photodegradation

pathways were further altered by the variation of different reactive species adsorbed

on the surface of electrode. Due to the existence of basic group on the GR/TNAs, the

isoelectric point of GR/TNAs was decreased compared to the TiO_2. The surface charge

of GR and TNAs could be totally opposite at certain pH, and strengthen the hybrid

structures of GR/TNAs via the strong electrostatic interaction[49].

3.2. Evaluation of the photocatalytic activity

The photocatalytic activities of GR/TNAs and TNAs photoelectrodes were evaluated

by the alachlor degradation. Fig. 11 shows the performance comparison of alachlor

degradation between GR/TNAs and TNAs photoelectrodes. The alachlor degradation

efficiency of both GR/TNAs and TNAs photoelectrodes increased with the increase of

reaction time from 0 to 60 min. Compared to the pure TNAs photoelectrodes, the

GR/TNAs photoelectrodes provided higher alachlor degradation efficiency at 0-40

min reaction time, suggesting that the introduction of GR could improve the

photocatalytic activity of TNAs. In order to evaluate the alachlor mineralization, the

TOC degradation efficiency was compared between the GR/TNAs and TNAs

photoelectrodes. As shown in Fig. 11, the TOC degradation efficiencies of TNAs and

GR/TNAs photoelectrodes increased by 55.29% and 64.63% at 60 min reaction time,

respectively. The results indicated that alachlor could be transformed into small

molecular substances, and these small molecular substances could be easily

biodegraded in the post treatment.

Compared to the TNAs photoelectrode, the GR/TNAs photoelectrodes had

higher photocatalytic activity and mineralization for alachlor, and it was could be

explained as follows: (1) the adsorption between alachlor and GR/TNAs

photoelectrodes could be remarkably driven by the giant two-dimensional π-π

conjugation structure of GR, which offers more reaction sites for the degradation

process[47, 50]. (2) The UV-vis DRS showed that the light utilization efficiency of

GR-doped TNAs was higher than TNAs. The electron could be more easily excited

from valence band to conduction band under the irradiation, and the photoelectron

accumulation on the GR surface and the holes on the TNAs surface happened during

the photocatalytic process. In addition, GR could strongly inhibit the charge

recombination and prolong the lifetime of the photongenerated electron-hole pairs due

to the Schottky barrier effect[12], which can promote the formation of reactive species

like $\cdot O_2^-$ and $\cdot OH$ for the alachlor degradation. Fig. 12 shows the photocatalytic

mechanism scheme of GR/TNAs photoelectrodes on the degradation of alachlor.

3.3. Effect of initial concentration on alachlor degradation

The effect of initial alachlor concentration on the alachlor degradation efficiency was

investigated at 2, 5, 6, 8 and 10 mg/L alachlor solution (Fig. 13). The alachlor

degradation efficiencies at different initial alachlor concentrations increased with the

increase of reaction time from 0 to 60 min. However, the alachlor degradation

efficiencies decreased with the increase of initial alachlor concentrations at 0-40 min

reaction time. For example, the alachlor degradation efficiencies at the initial

concentrations of 2, 5, 6, 8 and 10 mg/L were 98.7%, 96.2%, 92.9%, 90.1% and 85.6%

at 30 min reaction time, respectively. As shown in the inset of Fig. 10, the degradation

curves are fitted to the first-order kinetic law by using the following Langmuir–

Hinshelwood equation[51]:

$$-\ln(\frac{C_t}{C_0}) = kt \qquad\qquad (2)$$

where C_0 is the alachlor concentration of ad-desorption equilibrium, C_t is the alachlor

concentration at irradiation time t, and k is the first-order rate constant.

The alachlor concentrations of ad-desorption equilibrium for GR/TNAs were 1.91,

4.83, 5.8, 7.72 and 9.65 mg/L at the initial alachlor concentration of 2, 5, 6, 8 and 10

mg/L, respectively. The value of k for 2, 5, 6, 8 and 10 mg/L alachlor were calculated

as 15.1×10^{-2}, 12.0×10^{-2}, 9.9×10^{-2}, 8.7×10^{-2} and 8.2×10^{-2} min^{-1}, respectively.

The first-order rate constant decreased with the increase of initial alachlor

concentration. The active species such as ·OH and HO$_2$· were responsible for the

degradation of the alachlor during the photocatalysis process, which could be

generated with a limited total amount under the unchanged experimental conditions.

The number of active species per unit alachlor decreased with the increase of the

initial alachlor concentration, and then limited the catalytic reaction rate. Likewise,

the production of intermediate could also be promoted with the increase of the initial

alachlor concentration and led to the competition with alachlor for the adsorption site

and the consumption of active group. Additionally, the transparency of the solution

was relative low at a higher alachlor concentration, which resulted in the decrease of

the absorbed light intensity and light utilization efficiency[52].

3.4. Effect of pH on alachlor degradation

As pH can affect the banding state on the surface of photoelectrodes, it is regarded as an important parameter in the photodegradation process. The degradation efficiencies of alachlor were investigated at different initial pH values in the present experiment. As shown in Fig. 14, the photocatalytic activity of GR/TNAs decreased with the increase of initial pH. The first-order kinetic law was established in the inset of Fig. 14 by using the Langmuir–Hinshelwood equation. The first-order rate constants for pH values of 3, 4, 5, 7 and 11 were 17.8×10^{-2}, 17.0×10^{-2}, 14.1×10^{-2}, 12.6×10^{-2} and 12.1×10^{-2} min^{-1}, respectively, suggesting the k value decreased with the increase of initial pH value. The behavior of active species in the reaction process and chemical property of reactant were analyzed to explain the above-mentioned results as follows: (1) CO_2 producing from the photocatalytic reaction could be converted to the captors (e.g. CO_3^{2-} and HCO_3^-) for $\cdot$OH under the strong alkali environment, which could decrease the $\cdot$OH concentration and thus lead to adverse effects on the alachlor degradation. (2) The result of zeta potential illustrated that the surface of GR/TNAs was dominated by positive charges at pH less than 4.3, whereas the alachlor solution was negatively charged[53]. The negative charges were rich on the surfaces of both the electrode and alachlor at pH 4.3 or higher. The surface of GR/TNAs could attract more alachlor species at relatively low pH, whereas it repelled with the alachlor species at pH over 4.3. (3) The positive charges could accelerate the transportation of photo-generated electrons and suppress the charge recombination[54], which contributed to the generation of active species and then improved the degradation efficiency of

alachlor.

3.5. Effect of distance from illuminant on alachlor degradation

Fig. 15 shows the effect of the distance from the illuminant on the degradation efficiency of alachlor. The degradation efficiency of alachlor at the distance from the illuminant of 2, 4 and 6 cm were 99.92%, 91.83% and 70.87% under the conditions of initial alachlor concentration at 5 mg/L and xenon light irradiation for 1 h, respectively. The degradation efficiency of alachlor by GR/TNAs photoelectrodes gradually decreased with the increase of the distance from illuminant. As shown in the inserted figure in Fig. 12, the first-order rate constants were 12.0×10^{-2}, 4.1×10^{-2} and 2.1×10^{-2} min^{-1} for the distance of 2 cm, 4 cm and 6 cm from the illuminant, respectively, indicating that the k value decrease with the increase of illuminant distance. The increase of the light intensity could favor the generation of excited photoelectrons and accelerate the separation of electron-hole pairs[51]. The abundant electrons could be transformed to active oxygen species like $\cdot OH$ and $HO_2 \cdot$ and the remaining holes could produce the $\cdot OH$ via the interaction with $-OH$[42], which led to the higher degradation efficiency of alachlor and the increase of first-order rate constant.

3.6. Effect of anions on alachlor degradation

Many anions are generally existed in the nature water environment, which play important roles in the photocatalytic reaction. In order to investigate the effect of different anions on the degradation of alachlor, Cl^- (100 mg/L), NO_3^- (100 mg/L) and

SO_4^{2-} (100 mg/L) were chosen as the interfering ions in the present study. As shown

in Fig. 16, Cl^- exhibited a slight inhibition effect on the alachlor degradation, whereas

NO_3^- and SO_4^{2-} improved the photocatalysis efficiency. As Cl^- ion is known to be hole

scavengers, the reaction between the Cl^- and the positive holes on the surface of TiO_2

could reduce the degradation efficiency. Additionally, Cl^- could act as a strong

competitor to alachlor for the active species like $\cdot OH$, which was also responsible for

the prolonged degradation[55]. The specific reaction process was presented as follows[56]:

$$OX^{\bullet}+Cl^- \to Cl\cdot \quad \{radical\ scavenging\} \tag{3}$$

$$h_{vb}^{+}+Cl^- \to Cl\cdot \tag{4}$$

$$\cdot OH + Cl\cdot \to HOCl \tag{5}$$

$$Cl\cdot + Cl\cdot \to Cl_2 \tag{6}$$

Kim et al. reported that $\cdot OH$ could be produced by NO_3^- photolysis under the UV light

illumination and lead to the acceleration of photodegradation process[57]. The

mechanism of the generation is according to the Eq:

$$NO_3^- + hv \to NO_3^{-\bullet} \to NO_2^{-\ \bullet} + O^{\bullet} \tag{7}$$

$$O^{-\bullet} + H_2O \to OH^{\bullet} + OH^- \tag{8}$$

Concerning the positive effect of SO_4^{2-} on the photocatalysis, it might be ascribed to

the formation of the oxidizing radical species like $SO_4^{\bullet-}$, as shown in the following

Eq^{56}:

$$h_{vb}^{+} + SO_4^{2-} \to SO_4^{\bullet-} \tag{9}$$

However, the effect of Cl^-, NO_3^- and SO_4^{2-} on the photocatalytic reaction was

relatively low due to the initial neutral pH condition. As the zero point of charge of

GR/TNAs was about 4.3, negative charges were rich on the surface of the electrode at pH 7 and then the anions were repelled due to the electrostatic force, which weakened the interference of the anions on the photocatalysis.

3.7. Effect of cycle number on alachlor degradation

The stability of a photocatalyst is a significant indicator to evaluate its practical application. In order to evaluate the stability of GR/TNAs, the degradation efficiency of alachlor by GR/TNAs photocatalysis was investigated by recycling the photoelectrodes for 15 cycles under the xenon light irradiation for 60 min in each cycle. As shown in Fig. 17, GR/TNAs photoelectrodes maintained a satisfactory degradation efficiency of alachlor at above 99.5% for all cycles. The experimental results indicated an excellent chemical stability of GR/TNAs, which could be ascribed to the formation of robust coupling structure between GR and TNAs[38]. According to the aforementioned results in the present study, the introduction of GR could significantly accelerate the separation of photoelectron-hole pairs. The separated holes could be immediately captured by alachlor during the degradation, whereas the remained electrons could prevent the GR from oxidizing[14].

4. Conclusion

The GR/TNAs photoelectrodes had been successfully synthesized by the in-situ anodization and electro-deposition method. The as-prepared GR/TNAs photoelectrodes possessed a better photoelectric property than the bare TNAs. The introduction of GR had no obvious effect on the original crystallization of TNAs,

whereas the photoelectric property was significantly improved. The GR/TNAs

photoelectrodes also exhibited superb photocatalytic activity and chemical stability

for the alachlor degradation. After reusing the GR/TNAs photoelectrodes for 15 times,

the degradation efficiency could still be over 99.5%. The increase of the initial

concentration, initial pH or distance from the illuminant could suppress the alachlor

degradation. The photocatalysis could be enhanced by NO_3^- and SO_4^{2-}, whereas Cl^-

had a slight negative effect on the alachlor degradation. The enhancement of

photocatalytic performance by incorporating GR into TNAs will provided theoretical

basis for the practical application of GR/TNAs photoelectrodes.

Acknowledgements

References

1   M. V. Bagal and P. R. Gogate, *Sep. Purif. Technol.*, 2012, **90**, 92-100.

2   J. Qu, H. Li, H. Liu and H. He, *Catal. Today*, 2004, **90**, 291-296.

3   X. Wang and Y. Zhang, *J. Hazard. Mater.*, 2009, **161**, 202-207.

4   Z. Qiang, C. Liu, B. Dong and Y. Zhang, *Chemosphere*, 2010, **78**, 517-526.

5   D. Choi, O. M. Lee, S. Yu and S. W. Jeong, *J. Hazard. Mater.*, 2010, **184**, 308-312.

6   H. Katsumata, S. Kaneco, T. Suzuki, K. Ohta and Y. Yobiko, *J. Photoch. Photobio A*, 2006, **180**, 38-45.

7   J. Gomis, A. Arques, A. M. Amat, M. L. Marin and M. A. Miranda, *Appl. Catal. B- Environ.*, 2012, **123-124**, 208-213.

8   R. A. Torres, R. Mosteo, C. Petrier and C. Pulgarin, *Ultrason. Sonochem.*, 2009, **16**, 425-430.

9   N. Zhang, M.-Q. Yang, S. Liu, Y. Sun and Y.-J Xu, *Chem. Rev.*, 2015, **115**, 10307-10377

10   J. Wang, B. He and X. Z. Kong, *Appl. Surf. Sci.*, 2015, **327**, 406-412.

11   D. Rajamanickam, P. Dhatshanamurthi and M. Shanthi, *Spectrochim. Acta A*, 2015, **138**, 489-498.

12   Y. Zhang, Z. Zhou, T. Chen, H. Wang and W. Lu, *J. Environ. Sci-China*, 2014, **26**, 2114-2122.

13   D. S. Lee and S. J. Park, *Curr. Appl. Phys.*, 2015, **15**, 144-148.

14   Q. Zhang, N. Bao, X. Zhu, D. Ma and Y. Xin, *J. Alloy. Compd.*, 2015, **618**, 761-767.

15   J. Wang, P. Wang, Y. Cao, J. Chen, W. Li, Y. Shao, Y. Zheng and D. Li, *Appl. Catal. B- Environ.*, 2013, **136-137**, 94-102.

16   J. Hu, H. Li, Q. Wu, Y. Zhao and Q. Jiao, *Chem. Eng. J.*, 2015, **263**, 144-150.

17   C. Han, Z. Chen, N. Zhang, J. C. Colmenares and Y. J. Xu, *Adv. Funct. Mater.*, 2015, **25**, 221-229.

18   C. Liu, Y. Teng, R. Liu, S. Luo, Y. Tang, L. Chen and Q. Cai, *Carbon*, 2011, **49**, 5312-5320.

19   X. Liu, Y. Tang, S. Luo, Y. Wang, X. Zhang, Y. Chen and C. Liu, *J. Photoch. Photobio A*, 2013, **262**, 22-27.

20   M. Q. Yang, N. Zhang, M. Pagliaro and Y. J. Xu, *Chem. Soc. Rev.*, 2014, **43**, 8240-8254.

21   N. Zhang, Y. Zhang and Y. J. Xu, *Nanoscale*, 2012, **4**, 5792-5813.

22   Y. Chen, Y. Tang, S. Luo, C. Liu and Y. Li, *J. Alloy. Compd.*, 2013, **578**, 242-248.

23   S. Liu, Z. R. Tang, Y. Sun, J. C. Colmenares and Y. J. Xu, *Chem. Soc. Rev.*, 2015, **44**, 5053-5075.

24   Y. Zhang, Z. R. Tang, X. Fu and Y. J. Xu, *ACS Nano*, 2010, **4**, 7303-7314.

25   X. Q. An and J. C. Yu, *Rsc. Adv*, 2011, **1**, 1426-1434.

26   P. Roy, S. Berger and P. Schmuki, *Angew. Chem. Int. Edit.*, 2011, **5**0, 2904-2939.

27   Y. Zhang and C. Pan, *J. Mater. Sci.*, 2010, **46**, 2622-2626.

28 P. Dong, Y. Wang, L. Guo, B. Liu, S. Xin, J. Zhang, Y. Shi, W. Zeng and S. Yin, *Nanoscale*, 2012, **4**, 4641-4649.

29 D. Marcano, D. Kosynkin, J. Berlin, A. Sinitskii, Z. Sun, A. Slesarev, L. Alemany, W. Lu and J. Tour, *ACS Nano*, 2010, **4**, 4806-4814.

30 P. Wang, J. Wang, X. Wang, H. Yu, J. Yu, M. Lei and Y. Wang, *Appl. Catal. B-Environ.*, 2013, **132-133**, 452-459.

31 G. Jiang, Z. Lin, C. Chen, L. Zhu, Q. Chang, N. Wang, W. Wei and H. Tang, *Carbon*, 2011, **49**, 2693-2701.

32 G. Colón, M. C. Hidalgo, G. Munuera, I. Ferino, M. G. Cutrufello and J. A. Navío, *Appl. Catal. B- Environ.*, 2006, **63**, 45-59.

33 S. D. Perera, R. G. Mariano, K. Vu, N. Nour, O. Seitz, Y. Chabal and K. J. Balkus, *ACS Catal.*, 2012, **2**, 949-956.

34 X. Pu, D. Zhang, Y. Gao, X. Shao, G. Ding, S. Li and S. Zhao, *J. Alloy. Compd.*, 2013, **551**, 382-388.

35 M. Cao, P. Wang, Y. Ao, C. Wang, J. Hou and J. Qian, *Chem. Eng. J.*, 2015, **264**, 113-124.

36 X. Pan, Y. Zhao, S. Liu, C. L. Korzeniewski, S. Wang and Z. Fan, *ACS Appl. Mater. Inter.*, 2012, **4**, 3944-3950.

37 H.-i. Kim, G.-h. Moon, D. Monllor-Satoca, Y. Park and W. Choi, *J. Phys. Chem. C*, 2012, **116**, 1535-1543.

38 Y. Tang, S. Luo, Y. Teng, C. Liu, X. Xu, X. Zhang and L. Chen, *J. Hazard. Mater.*, 2012, **241-242**, 323-330.

39   H. F. Zhuang, C. J. Lin, Y. K. Lai, L. Sun and J. Li, *Environ. Sci. Technol.*, 2007,

41, 4735-4740.

40   K. Zhou, Y. Zhu, X. Yang, X. Jiang and C. Li, *New J. Chem.*, 2011, **35**, 353.

41   K. Li, J. Xiong, T. Chen, L. Yan, Y. Dai, D. Song, Y. Lv and Z. Zeng, *J. Hazard.

Mater.*, 2013, **250-251**, 19-28.

42   Y. Xin, H. Liu, L. Han and Y. Zhou, *J. Hazard. Mater.*, 2011, **192**, 1812-1818.

43   M. Q. Yang, N. Zhang and Y. J. Xu, *ACS Appl. Mater. Inter.*, 2013, **5**,

1156-1164.

44   X. Song, J. Wu, M. Tang, B. Qi and M. Yan, *J. Phys. Chem. C*, 2008, **112**,

19484-19492.

45   H. Zhang, R. Zhong, J. Zhao and Y. Zhu, *Environ. Sci. Technol.*, 2008, **42**,

3803-3807.

46   N. Zhang, Y. Zhang, X. Pan, M. Q. Yang and Y. J. Xu, *J. Phys. Chem. C*, 2012,

116, 18023-18031.

47   H. Zhang, X. Lv, Y. Li, Y. Wang and J. Li, *ACS Nano*, 2010, **4**, 380-386.

48   S. Sun, L. Gao and Y. Liu, *Appl. Phys. Lett.*, 2010, **96**, 083113-1-083113-3.

49   S. Yang, X. Feng, S. Ivanovici and K. Mullen, *Angew. Chem. Int. Edit.*, 2010, **49**,

8408-8411.

50   Q. Li, B. Guo, J. Yu, J. Ran, B. Zhang, H. Yan and J. R. Gong, *J. . Am.Chem.

Soc.*, 2011, **133**, 10878-10884.

51   W.Y. Wang, M.L. Yang and Y. Ku, *Chem. Eng. J.*, 2010, **165**, 273-280.

52   Y. Li, X. Duan, X. Li and D. Zhang, *Mar. pollut. Bull.*, 2013, **66**, 47-52.

53   K. Wantala, P. Khemthong, J. Wittayakun and N. Grisdanurak, *Korean J. Chem. Eng.*, 2011, **28**, 2178-2183.

54   H. Zhao, S. Xu, J. Zhong and X. Bao, *Catal. Today*, 2004, **93-95**, 857-861.

55   A. K. Gupta, A. Pal and C. Sahoo, *Dyes Pigments*, 2006, **69**, 224-232.

56   P. Surolia, R. Tayade and R. Jasra, *Ind. Eng. Chem. Res.*, 2007, **46**, 6196-6203.

57   M. K. Kim and K. D. Zoh, *Sci. Total Environ.*, 2013, **449**, 95-101.
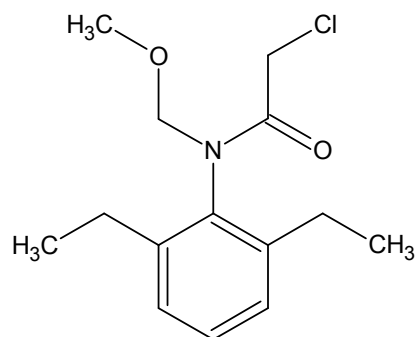
Fig. 1 Structure of alachlor
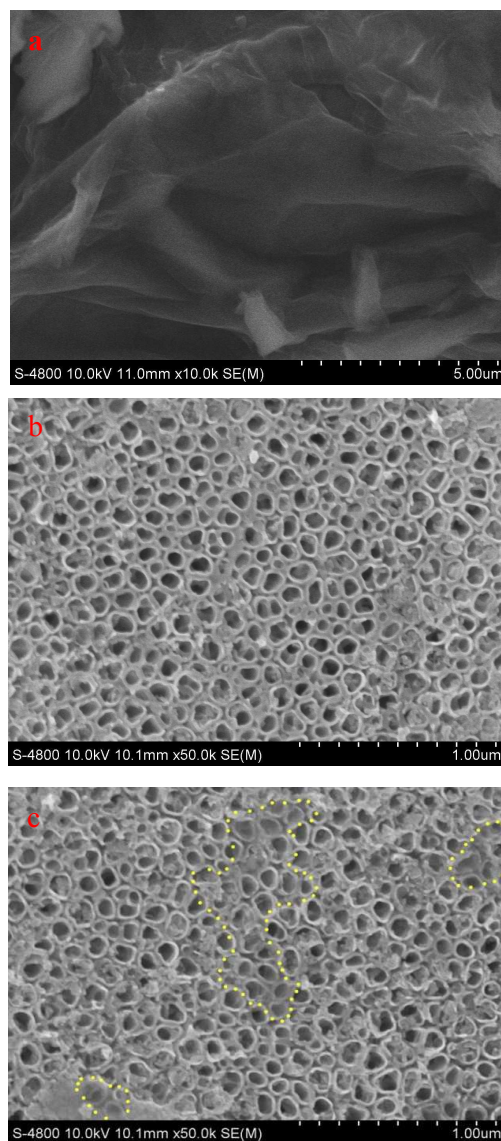
Fig. 2 SEM images of GR (a), TNAs (b) and GR/TNAs photoelectrodes (c). Partial GR islands are marked by the dots for the eye guide.
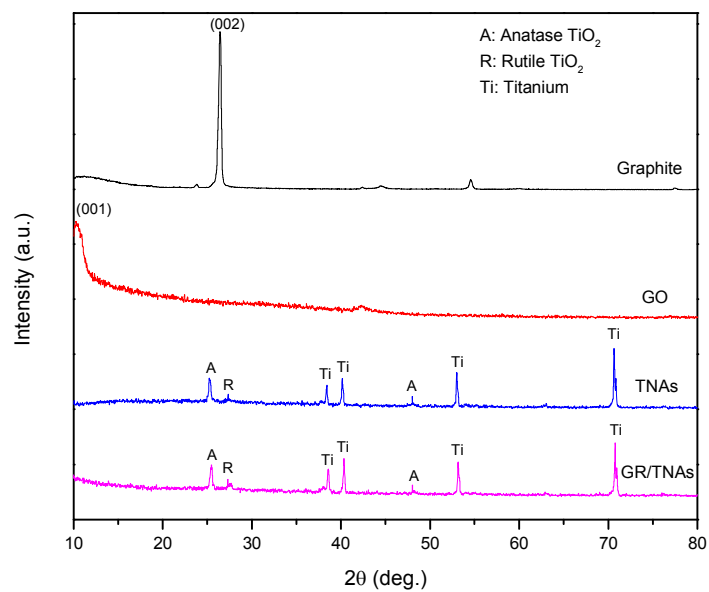
Fig. 3 XRD patterns of graphite, GO, TNAs and GR/TNAs photoelectrodes.
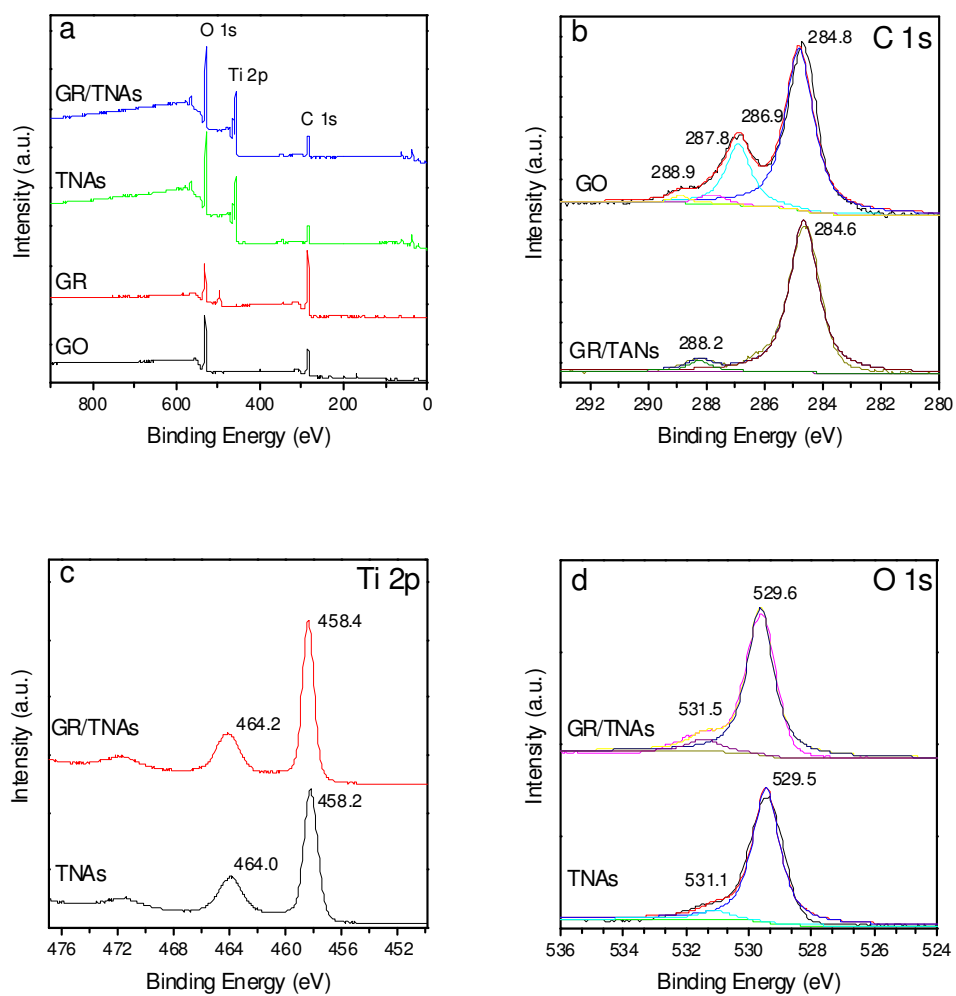
Fig. 4 (a) XPS survey spectra of GO, GR, TNAs and GR/TNAs; (b) C 1s spectra of GO and GR/TNAs; (c) Ti 2p spectra of TNAs and GR/TNAs; (d) O 1s spectra of TNAs and GR/TNAs.
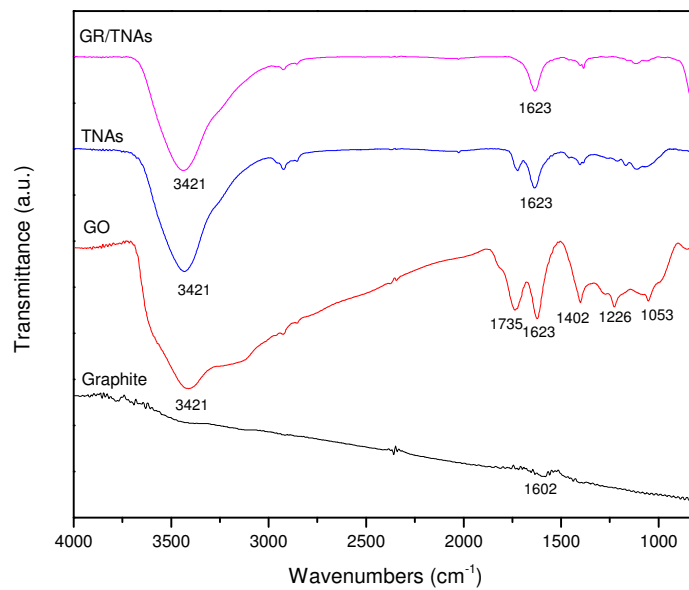
Fig. 5 FTIR spectra of graphite, GO, TNAs and GR/TNAs photoelectrodes.
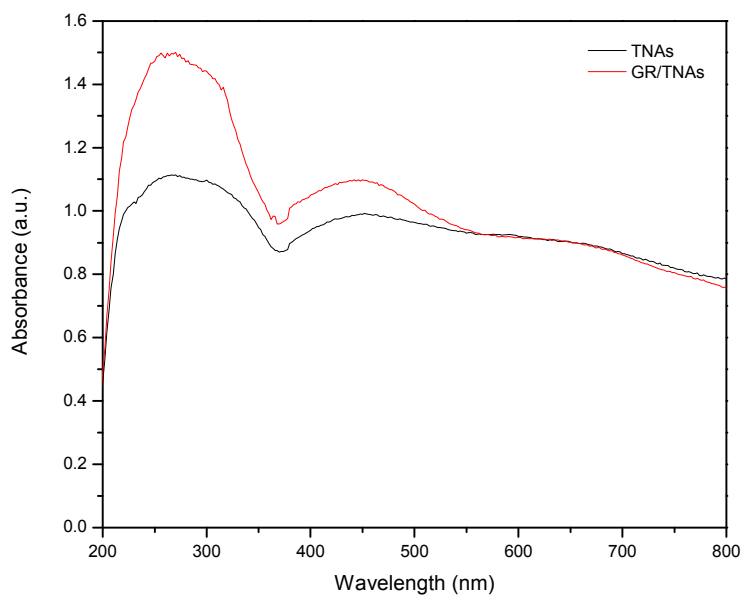
Fig. 6 UV–vis absorption spectra of TNAs and GR/TNAs photoelectodes.
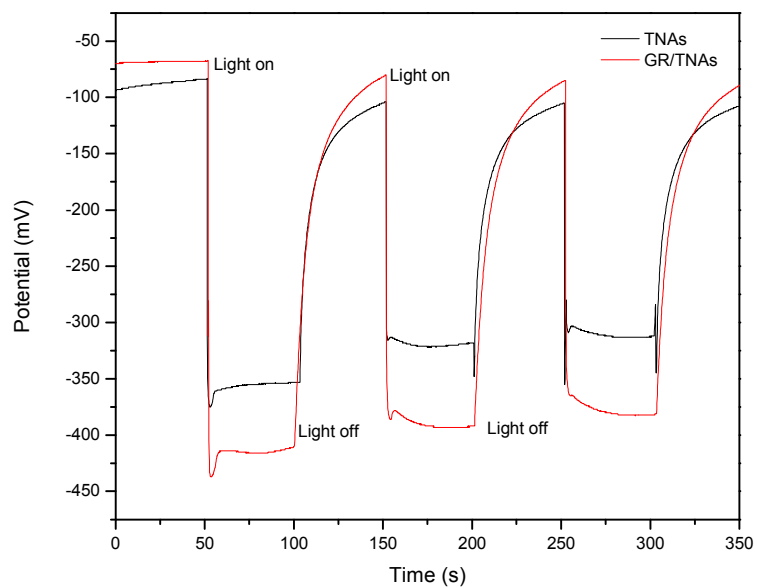
Fig. 7 Photovoltage responses of TNAs and GR/TNAs photoelectrodes under open-circuit condition.
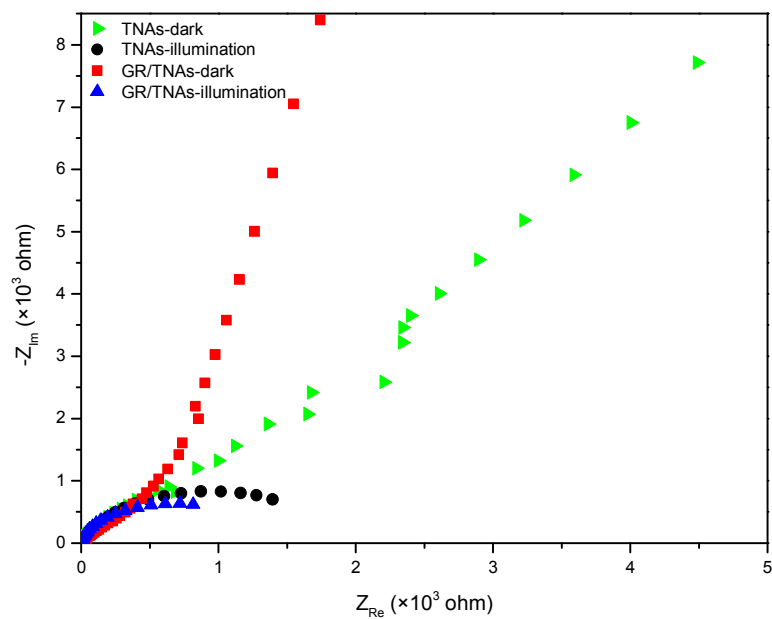
Fig. 8 EIS Nyquist plots of TNAs and GR/TNAs photoelectrodes with and without illumination.
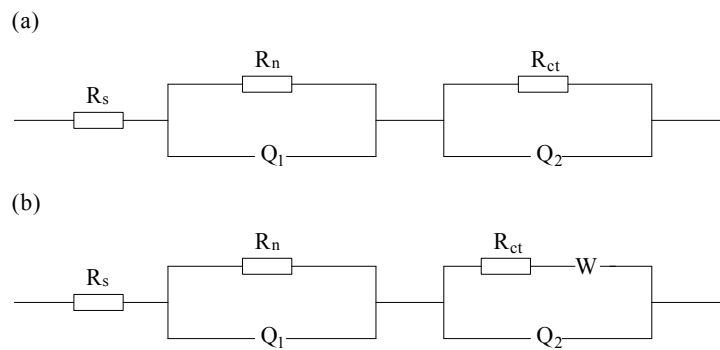
Fig. 9 Typical equivalent circuit for the TNAs and GR/TNAs photoelectrode: (a) under xenon light illumination and (b) in the dark.
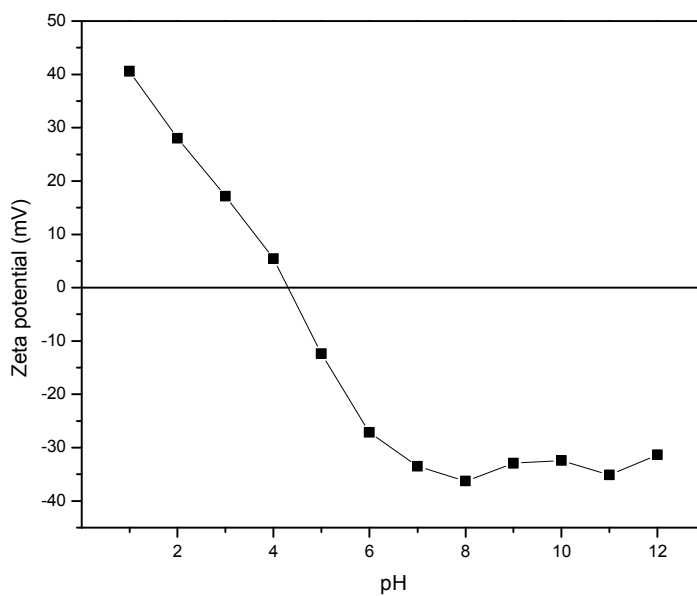
Fig. 10 Zeta potential as a function of pH for GR/TNAs photoelectrode.
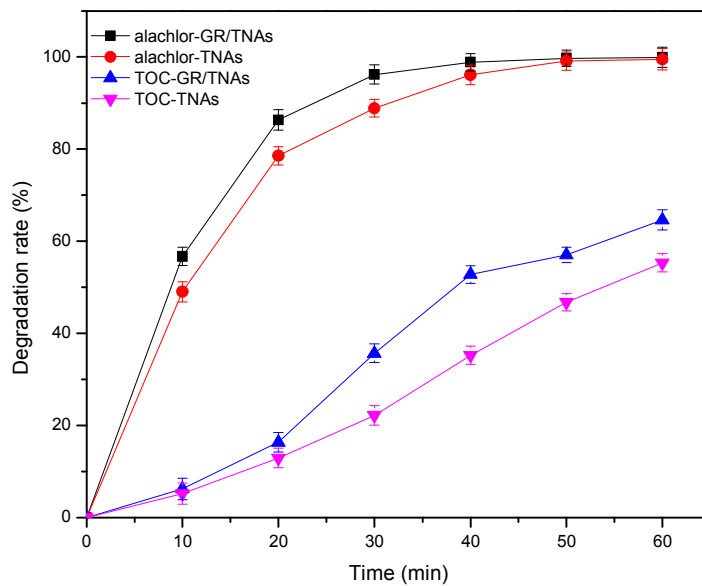
Fig. 11 Photodegradation of alachlor and TOC by TNAs and GR/TNAs photoelectrodes (5 mg/L

alachlor, pH=7, 25℃, and 3 cm from illuminant).
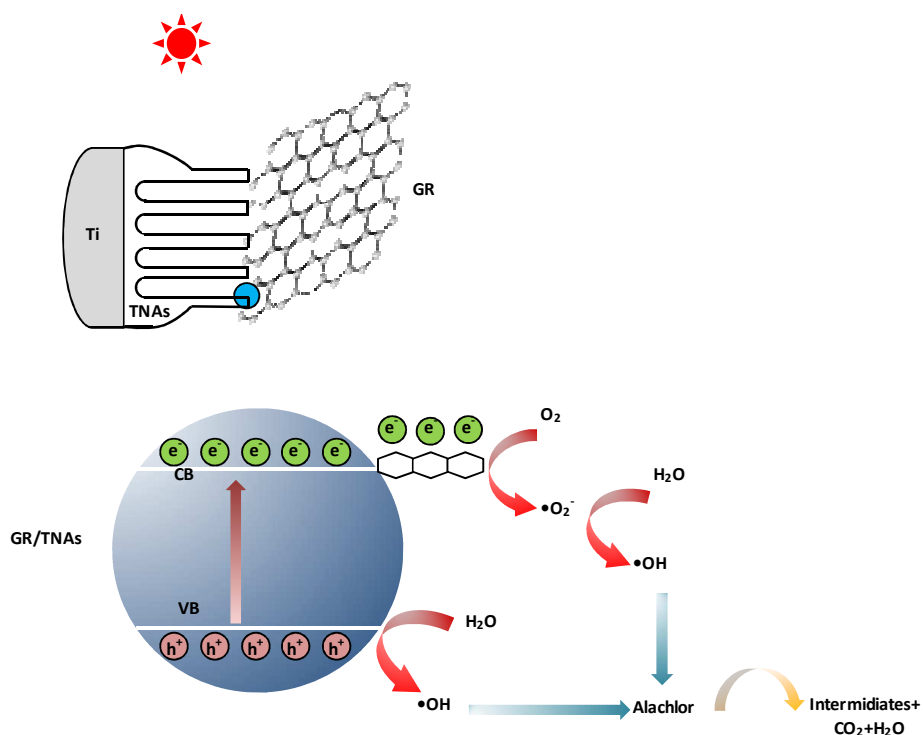
Fig. 12 Photocatalytic mechanism scheme of GR/TNAs photoelectrodes on the degradation of alachlor
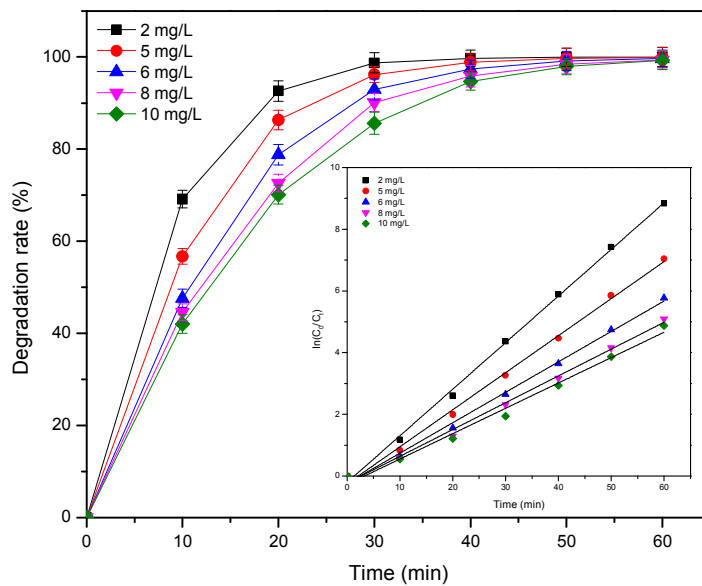
Fig. 13 Photodegradation of alachlor by GR/TNAs photoelectrodes at different initial

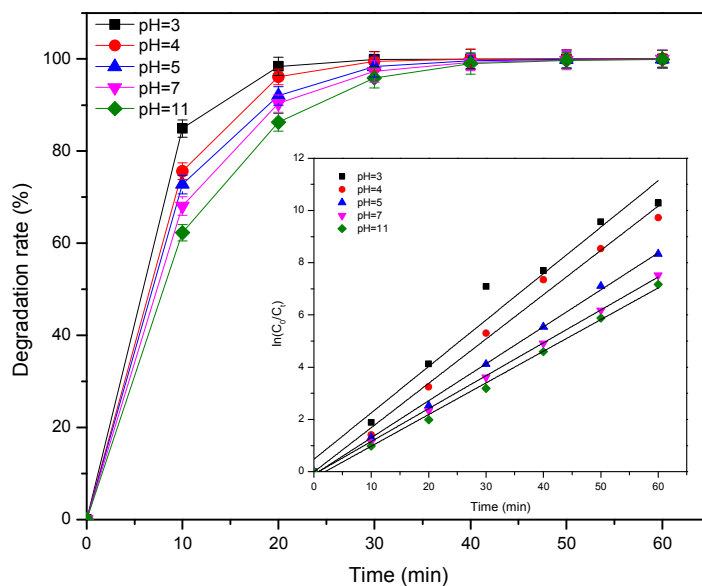concentration (pH=7, 25 ℃, and 3 cm from illuminant) and first-order fitting curves (inset).

Fig. 14 Photodegradation of alachlor by GR/TNAs photoelectrodes at different pH values (5 mg/L

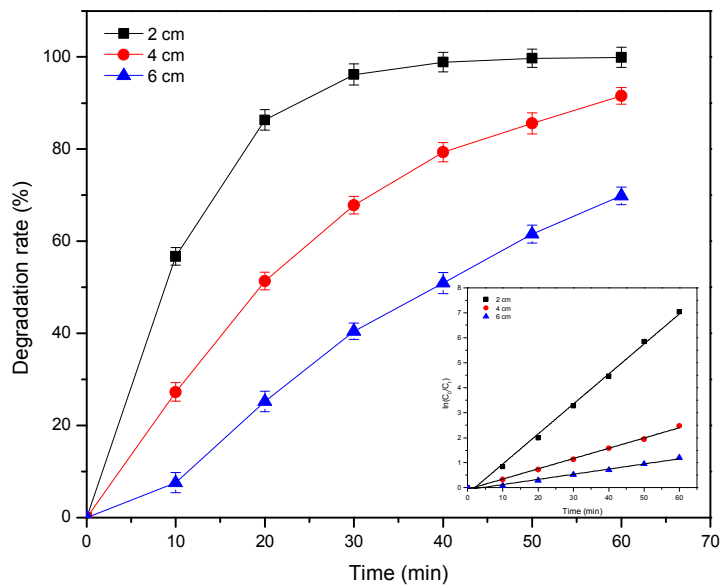alachlor, 25℃, and 3 cm from illuminant) and first-order fitting curves (inset).

Fig. 15 Photodegradation of alachlor by GR/TNAs photoelectrodes in the presence of different distance from illuminant (5 mg/L alachlor, pH=7, and 25℃) and first-order fitting curves (inset).
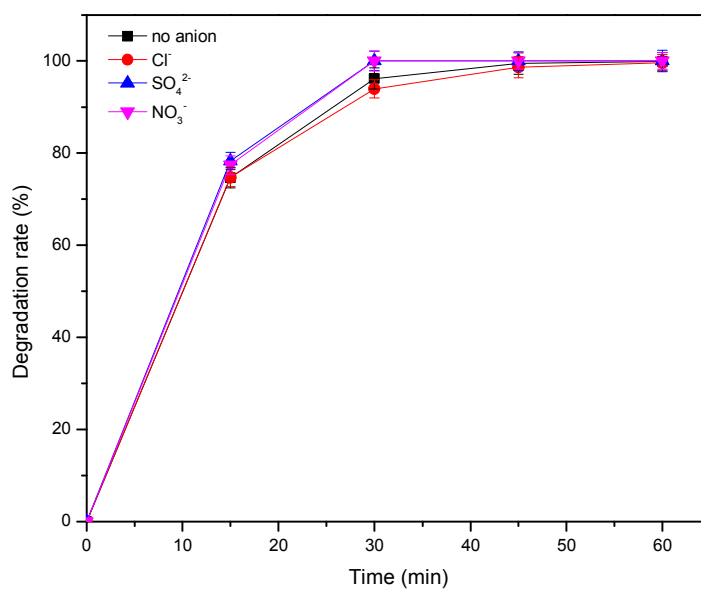
Fig. 16 Photodegradation of alachlor by GR/TNAs photoelectrodes in the presence of different anions (5 mg/L alachlor, pH=7, 25℃, and 3 cm from illuminant).
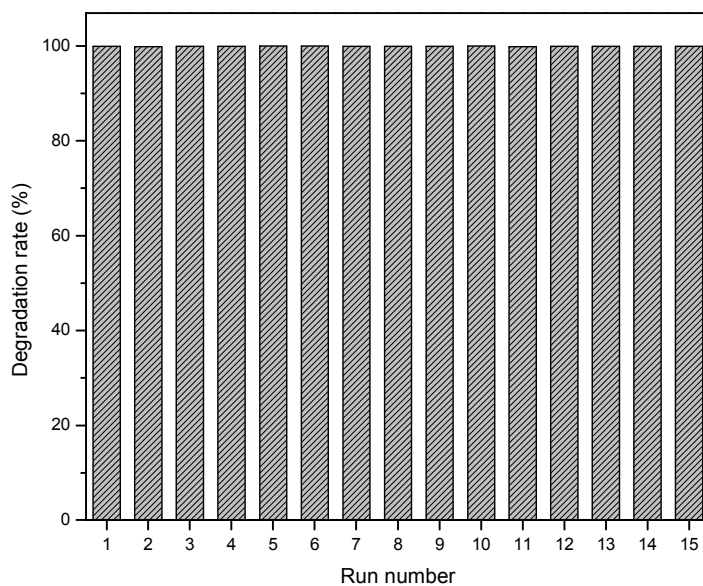
Fig. 17 Photodegration of alachlor by GR/TNAs photoelectrodes with 15 successive cycles under 60 min of xenon light illumination for each cycle.